IMPERIAL

TotalEnergies

# Generalized Network Modelling of Displacement in Multiscale Carbonates

Asli S. Gundogar, Anindityo Patmonoaji, Sajjad Foroughi, Martin J. Blunt, Branko Bijeljic

**Imperial College Consortium on Pore Scale Modelling and Imaging**
**Annual Meeting**

15 January 2025

# Motivation

*Unresolved = sub-resolution = microporosity*

- **Generalized Network Modeling (GNM)**
  - Richer geometry than classical networks
  - Connectivity through corners
  - 3D interfacial curvature in both axial and sagittal planes (**Giudici et al., *Water Resour. Res.*, 2023**)
  - Corner conductivity using direct numerical simulations
  - Computationally efficient

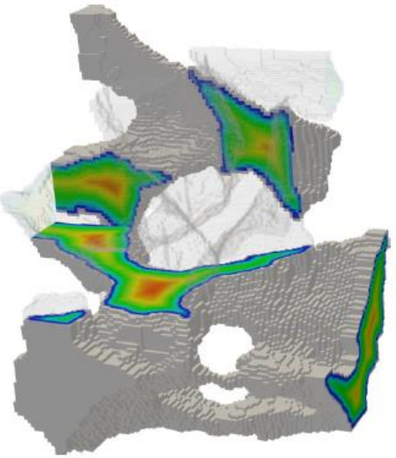

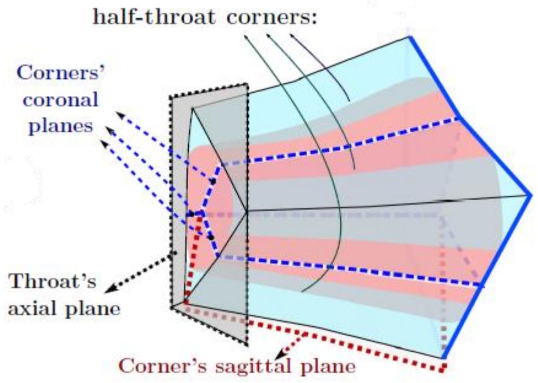


**(Raeini et al., *Phys. Rev. E.*, 2017; 2018)**

- **Multiscale carbonates**
  - Wide pore size distribution with intricate connectivity
  - A single image fails to capture the full range of connected (percolating) porosity
  - Sub-resolution porosity critical for interconnectivity
  - **Size/resolution trade-off**

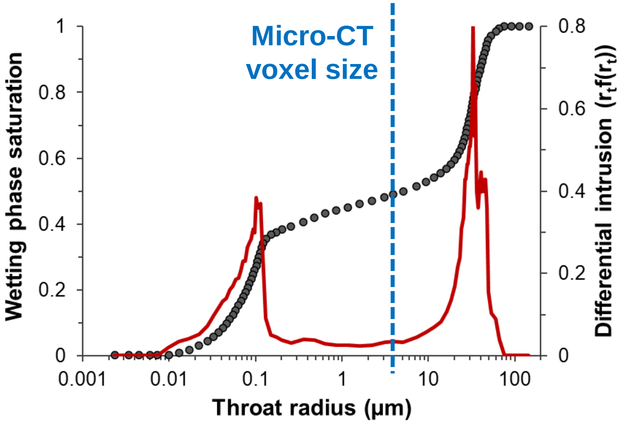


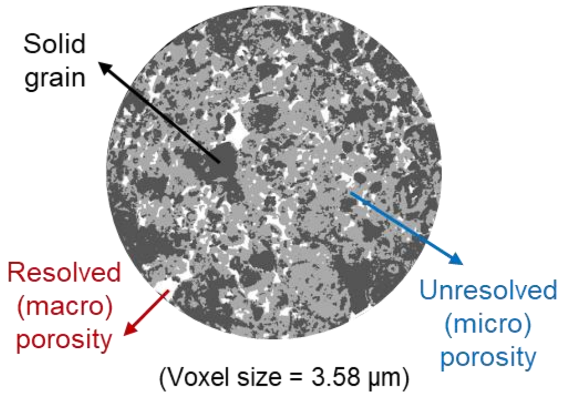


- **Our aim is to develop a multiscale GNM that incorporates sub-resolution porosity through differential imaging, enhancing predictive capabilities and elucidating the interplay between macroporosity and unresolved porosity on transport properties in a computationally efficient manner.**

# Multiscale (dual) network approaches

- Integrating networks from μCT images at different resolutions for two-scale pore network construction (Sok et al. 2010; Jiang et al. 2013; Mehmani and Prodanović, 2014; Prodanović et al. 2015; Pak et al. 2016)
- Treating microporous regions as a porous continuum rather than as discrete pores (Ioannidis and Chatzis, 2000; Bekri et al. 2005; Bauer et al. 2012; Bultreys et al. 2015)
- Connected microporosity using μCT scans of dry and contrast X-ray attenuating fluid-saturated samples (Bultreys et al. 2016; Ruspini et al. 2021; Wang et al. 2022; Foroughi et al. 2024)

**Multiscale network fusion**

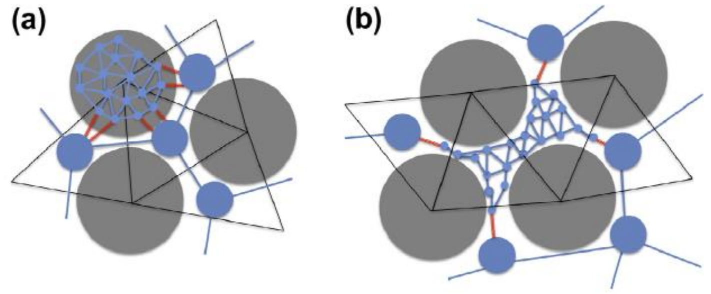


Mehmani and Prodanović, *Adv. Water Resour.*, 2014

**Microporosity as continuous medium**

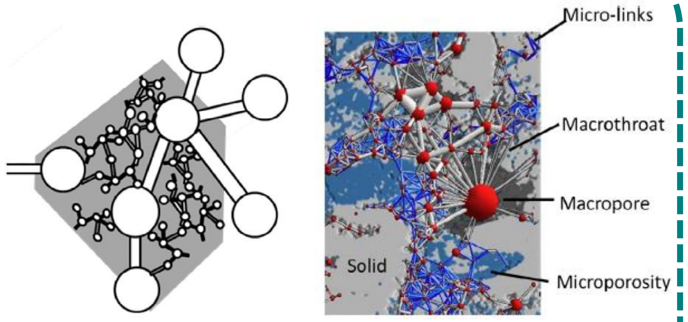


Bultreys et al., *Adv. Water Resour.*, 2015

**Effective microporosity**

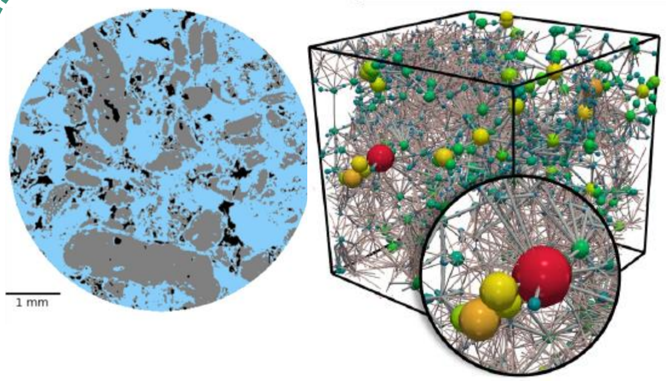


Foroughi et al., *WRR*, 2024

- **excludes isolated pore clusters**
- **significantly less computational load**

# Microlink identification using X-ray differential imaging

- Multiscale GNM with unresolved porosity through microlinks

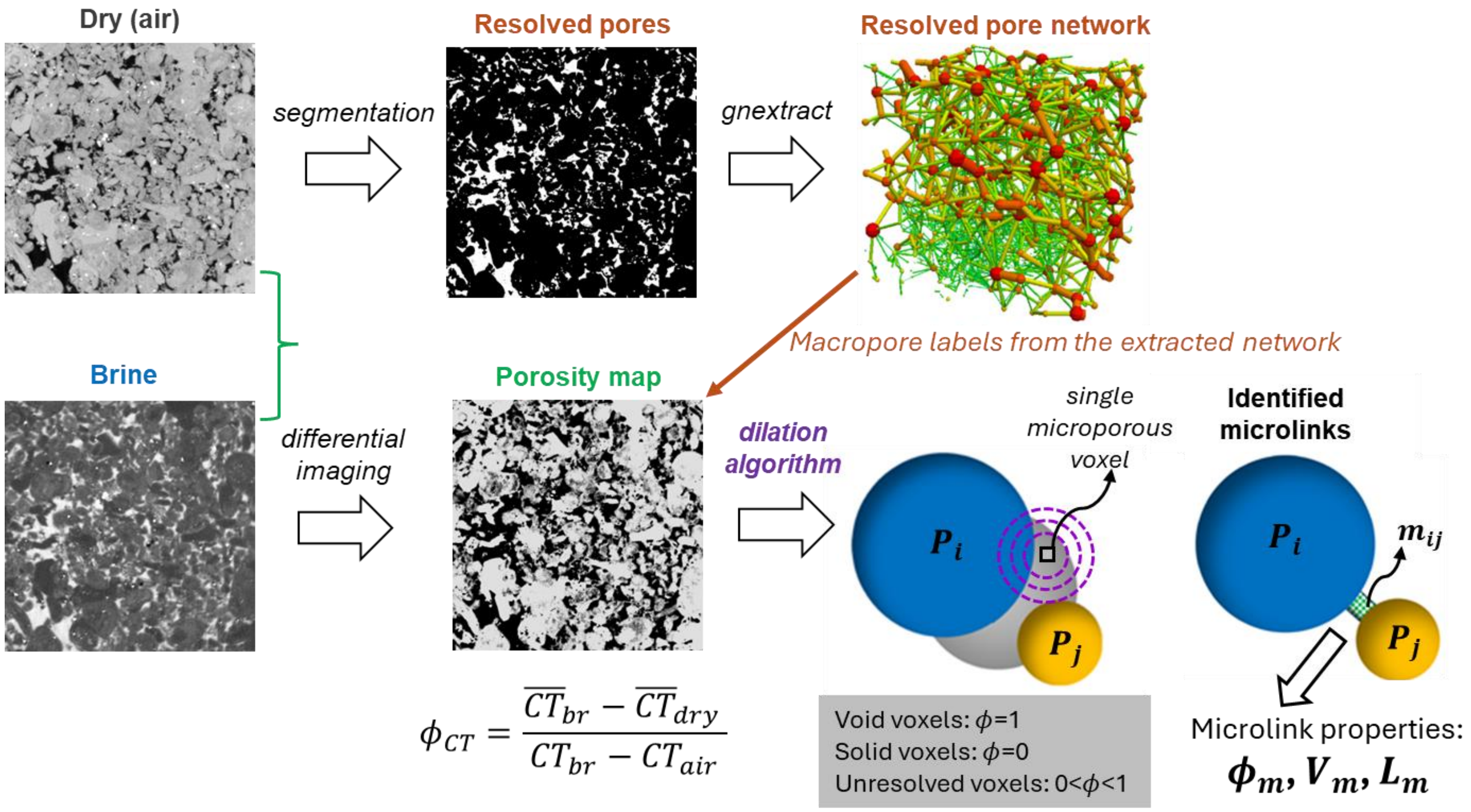


**Model inputs:**

- Connected pore indices ($P_i, P_j$)
- Pore volume ($V_m^p$)
- Length ($L_m$)
- Cross-sectional area ($A_m = \eta \frac{V_m}{L_m}$)
- Average porosity ($\phi_m$)
- Permeability ($K_m$)

- **Foroughi, S., Bijeljic, B., Gao, Y., & Blunt, M. J. (2024). Incorporation of sub-resolution porosity into two-phase flow models with a multiscale pore network for complex microporous rocks. *Water Resources Research*, 60(4), e2023WR036393.**

# Modeling drainage in microlinks

- Empirical relations are used to model flow in microlinks with Darcy-type porous medium:

**Absolute permeability (Kozeny-Carman equation):**

$$K_m = \frac{1}{180} \frac{\phi_m^3\, \boldsymbol{d_g^2}}{(1-\phi_m)^2}$$

$\boldsymbol{d_g}$: grain diameter

**Mass conservation at every pore center:**

$$\sum_{t \in i} q_t = \boldsymbol{g_t}(P_i - P_j) = 0$$

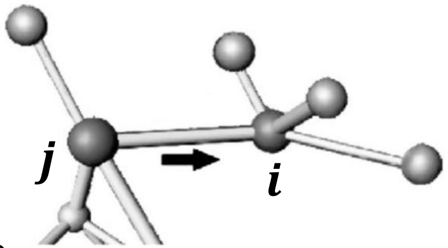


**Darcy's law for flow conductance:**

$$g_{p,m}^q = \frac{K_m k_{rp}(S_w)}{\mu_p} A_m$$

$\boldsymbol{p}$: fluid phase

**Archie's law for electrical conductance:**

$$g_{w,m}^e = \frac{S_w^n}{FF \times R_w} A_m \quad \text{where} \quad FF = \frac{R_o}{R_w} = \frac{a}{\phi_m^b}$$

$R_w$: water resistivity

$\boldsymbol{a}$: tortuosity factor

$\boldsymbol{b}$: cementation exponent

**Leverett J-function:**

$$J(S_w) = \frac{P_c(S_w)}{\sigma \cos\theta} \sqrt{K_m / \phi_m}$$

**Brooks-Corey $P_c$ model:**

$$J(S_w) = \boldsymbol{J_i}\, S_e^{-1/\boldsymbol{\lambda}} \rightarrow S_e = \left(J_i / J\right)^{\boldsymbol{\lambda}}$$

$\boldsymbol{J_i}$: initial J-value

$\boldsymbol{\lambda}$: saturation exponent

**Normalized water saturation:**

$$S_e = \frac{S_w - S_{wr}}{1 - \boldsymbol{S_{wr}}} \rightarrow S_w = S_e(1 - S_{wr}) + S_{wr}$$

**Brooks-Corey $k_r$ model:**

$$k_{rw}(S_w) = k_{rw}^{max}\, S_e^{\alpha_w}$$

$$k_{ro}(S_w) = k_{ro}^{max}(1 - S_e)^{\alpha_o}$$

$\boldsymbol{k_{rw}^{max}}, \boldsymbol{k_{ro}^{max}}$: endpoint $k_r$

$\boldsymbol{\alpha_w}, \boldsymbol{\alpha_o}$: power-law exponents

$\boldsymbol{d_g, \eta}$ → ***tuning parameters for measured permeability and formation factor***

$\boldsymbol{\lambda, J_i, d_g, S_{wr}}$ → ***adjustable parameters for drainage $P_c$ behavior***

# Multiscale experiments for model validation

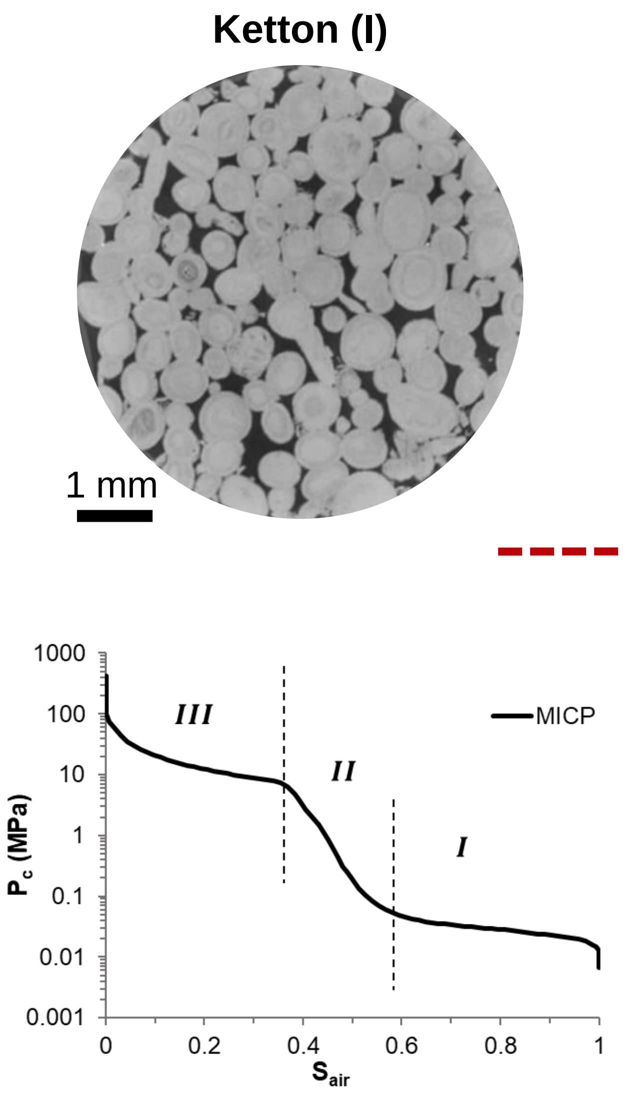


Mercury injection Pc data
(Tanino and Blunt, 2012)

*Increase in heterogeneity*

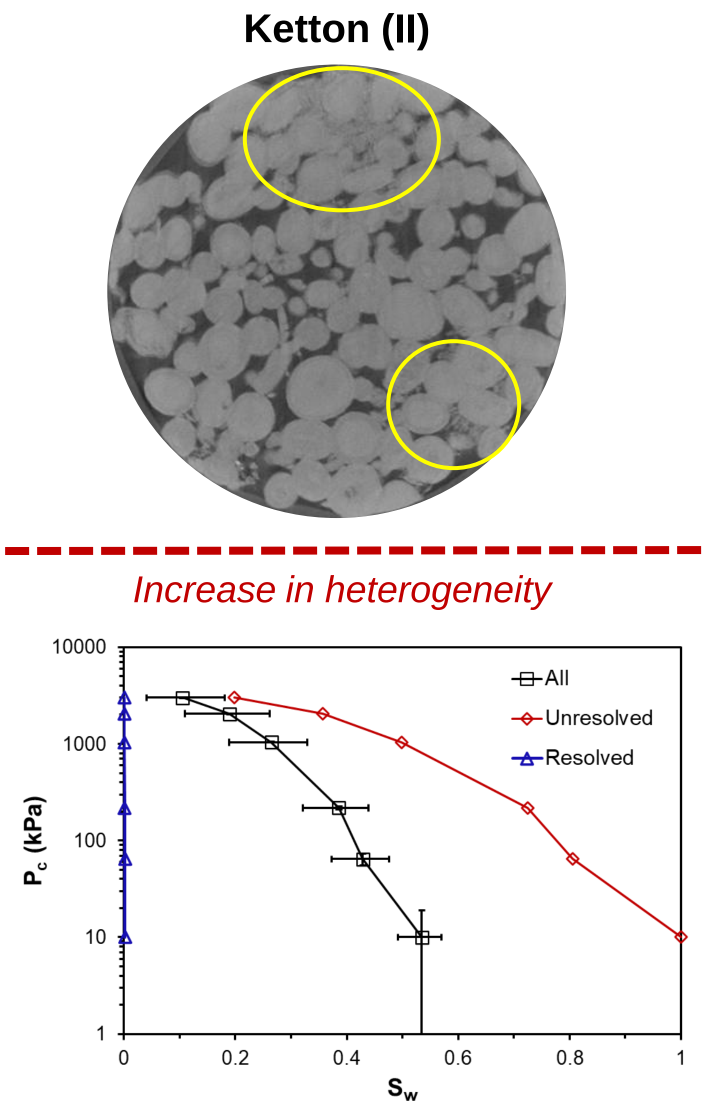


Porous plate displacement experiment
(Patmonoaji et al. *Under review*)

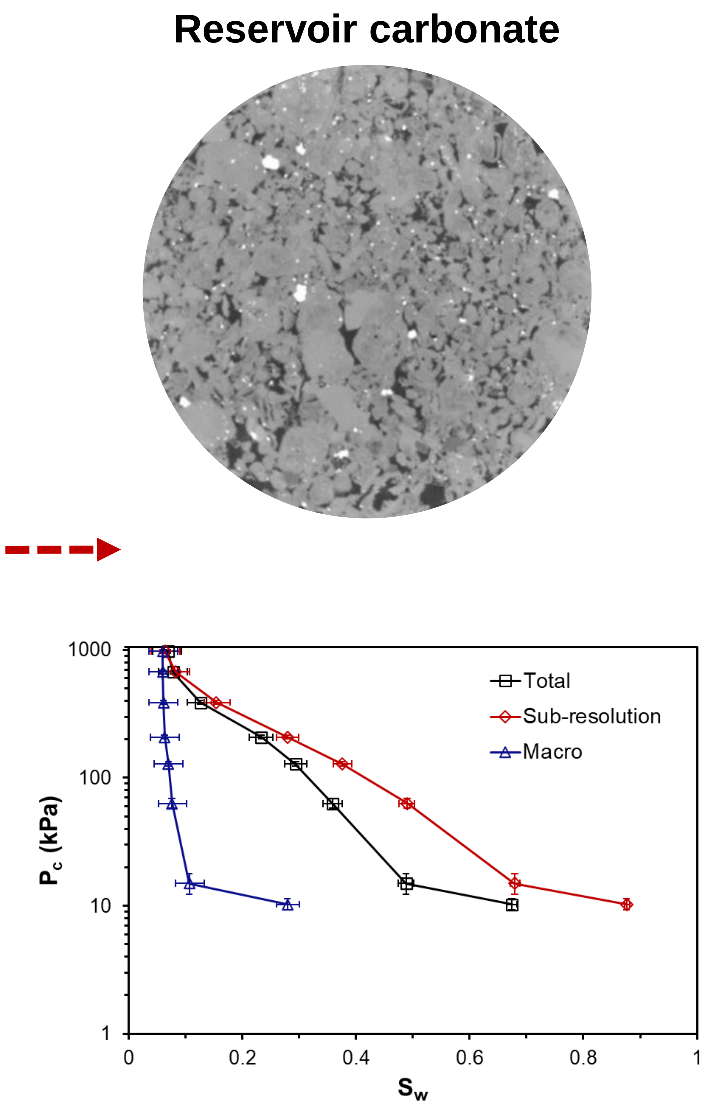


Porous plate displacement experiment
(Zhang et al., *J. Hydrol*, 2023)

# Ketton(I) sample (Zhang et al. 2023a)

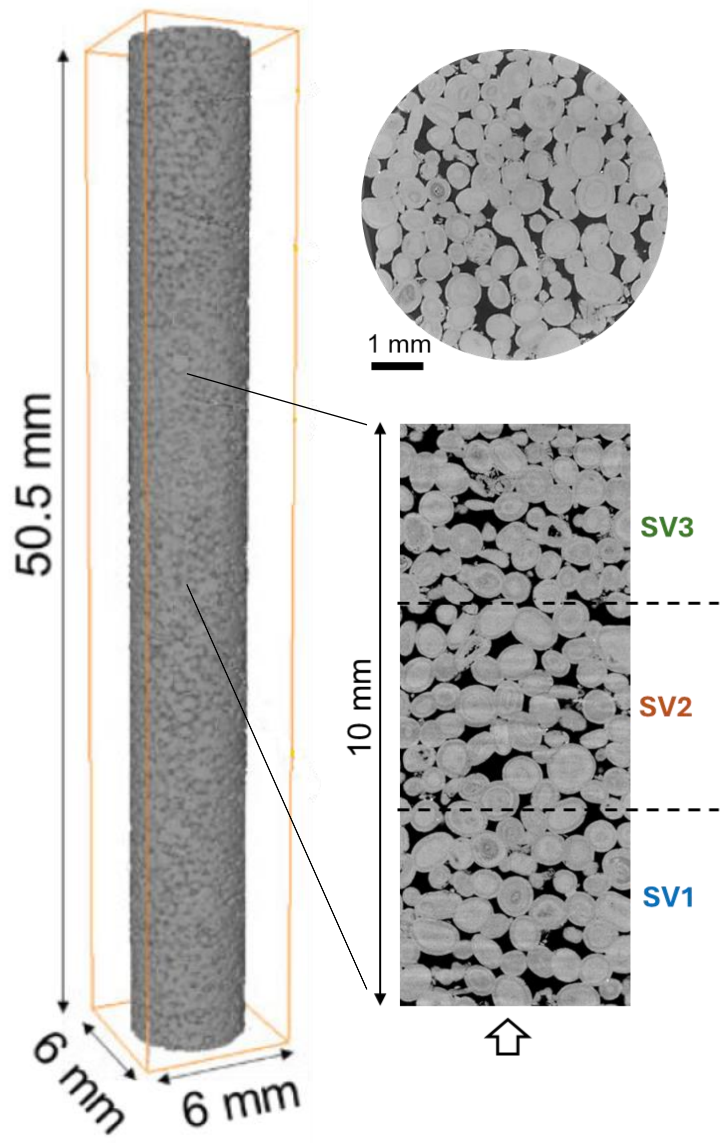


- A permeable, calcite-rich Ketton oolitic limestone
  - **Helium porosity** = 0.239
  - **Micro-CT porosity** = 0.236
  - **Brine permeability** = 2.45 D
- Microlink determination for three sub-volumes (**$1100^3$ voxels**)
- Distinct porosity regions characterized by mercury injection Pc (MICP) data:

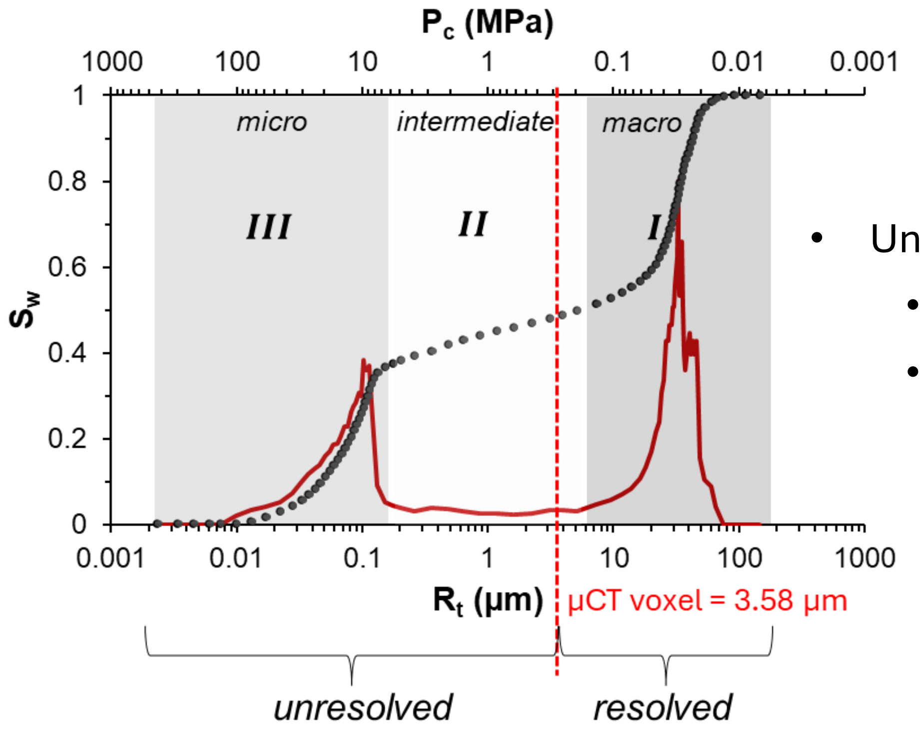


- Unresolved porosity covers
  - intermediate-sized and
  - microporosity regions

# Ketton(I) sample (Zhang et al. 2023a)

- MICP data is used to anchor the multiscale GNM for Ketton(I)

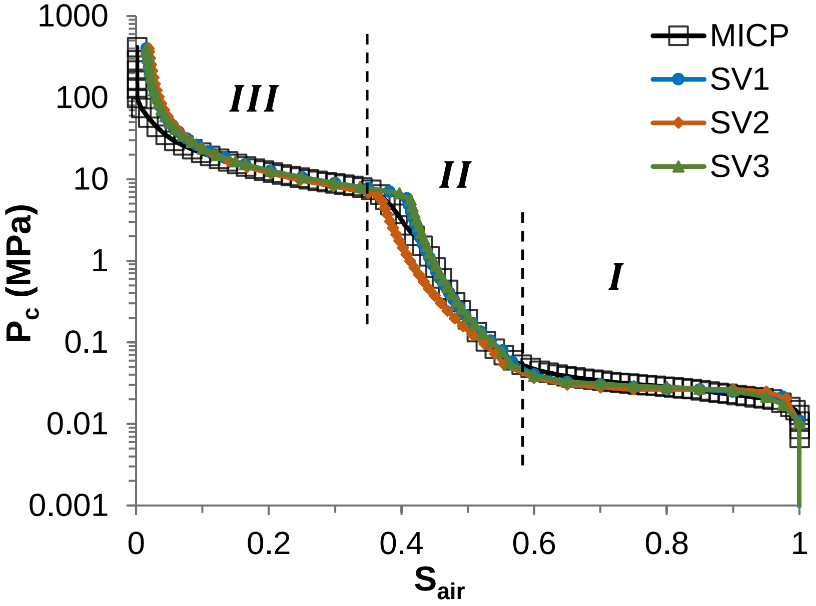


**Tuning parameters:**

| | |
|---|---|
| $d_g$ | $\begin{cases} 40\ \mu m & \phi_m > 0.155 \\ 0.6\ \mu m & \phi_m \le 0.155 \end{cases}$ |
| $J_i$ | 0.1 |
| $\lambda$ | $\begin{cases} 0.3 & \phi_m > 0.155 \\ 1.4 & \phi_m \le 0.155 \end{cases}$ |

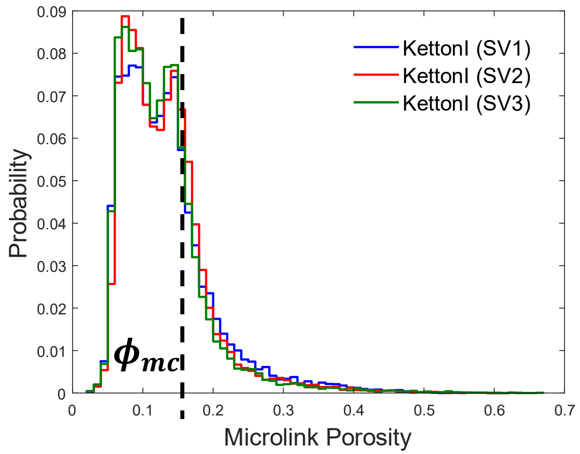


| | Resolved | | | Multiscale | | |
|---|---|---|---|---|---|---|
| | SV1 | SV2 | SV3 | SV1 | SV2 | SV3 |
| $N_p$ | 3299 | 2838 | 2797 | 3299 | 2838 | 2797 |
| $N_t$ | 5905 | 5232 | 5184 | 5905 | 5232 | 5184 |
| $N_{mL}$ | – | – | – | 22047 | 18529 | 19127 |
| $Z$ | 1.79 | 1.84 | 1.85 | 8.47 | 8.37 | 8.69 |
| $\phi$ | **0.137** | **0.141** | **0.138** | **0.236** | **0.234** | **0.235** |
| $K$ [mD] | 6065 | 7221 | 6690 | 6291 | 7567 | 6920 |
| $FF$ | 26.2 | 23.6 | 24.7 | 5.9 | 5.5 | 5.6 |

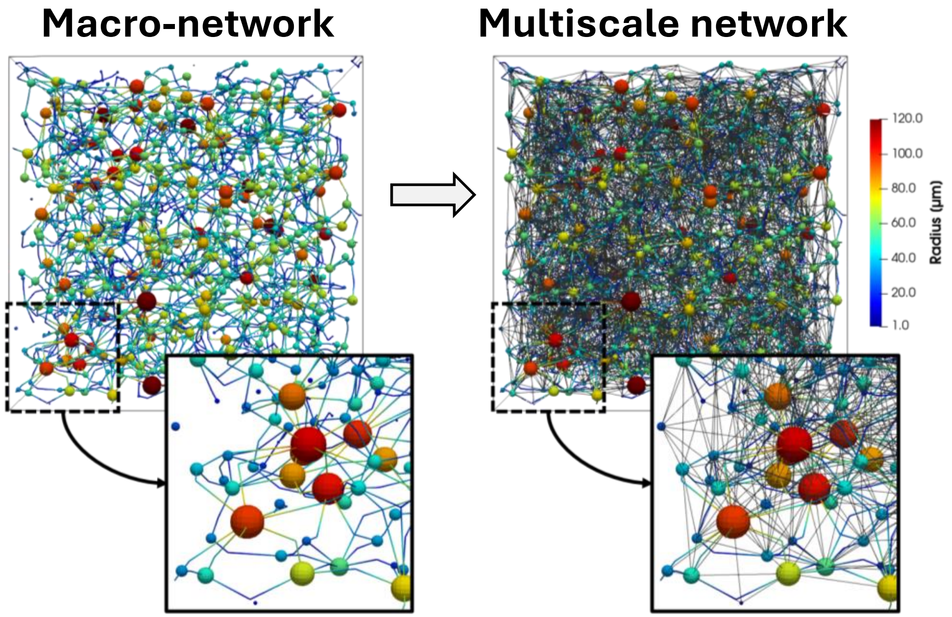

# Ketton(I) sample (Zhang et al. 2023a)

- Multiscale GNM drainage results for the sub-volumes (SV):

***As sample permeability increases, $k_r$ cross point shifts to the left***

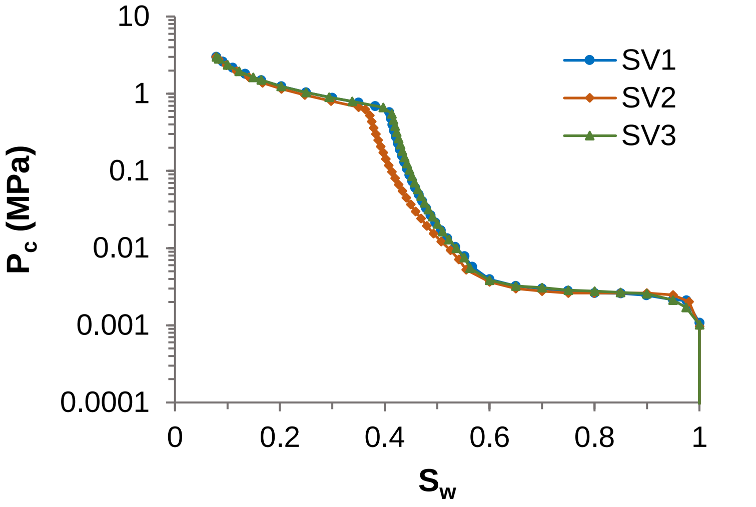


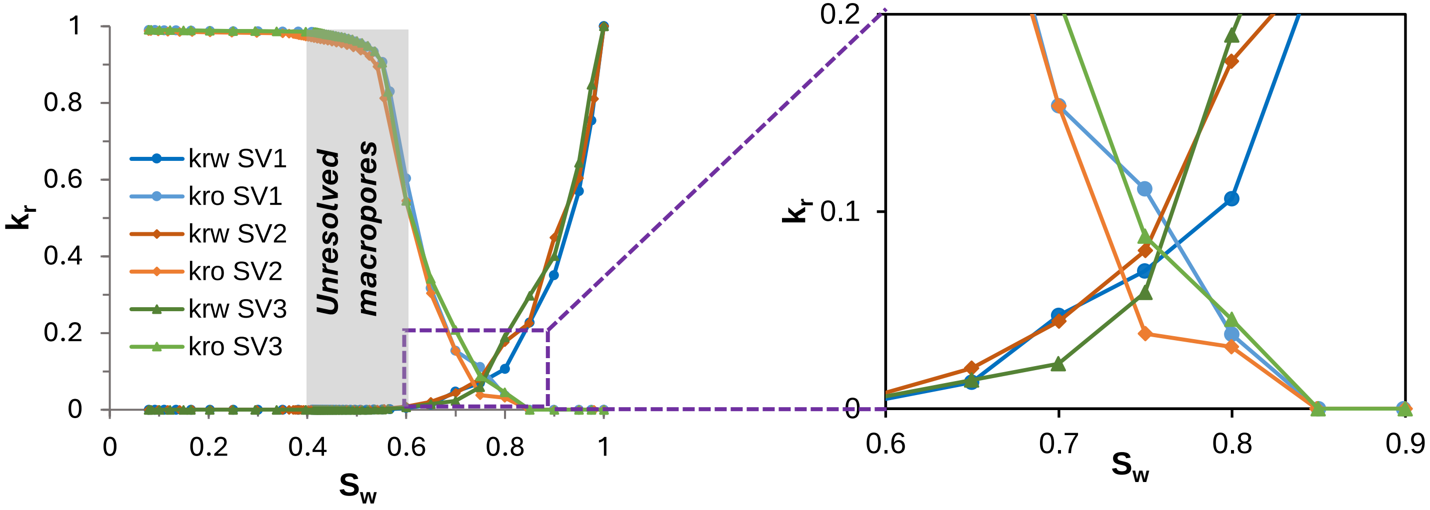


- Resolved (single-scale) GNM drainage results for the sub-volumes:

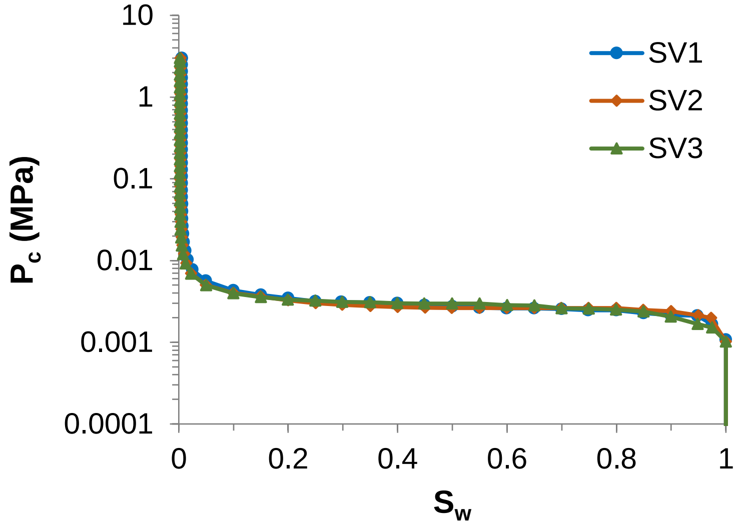


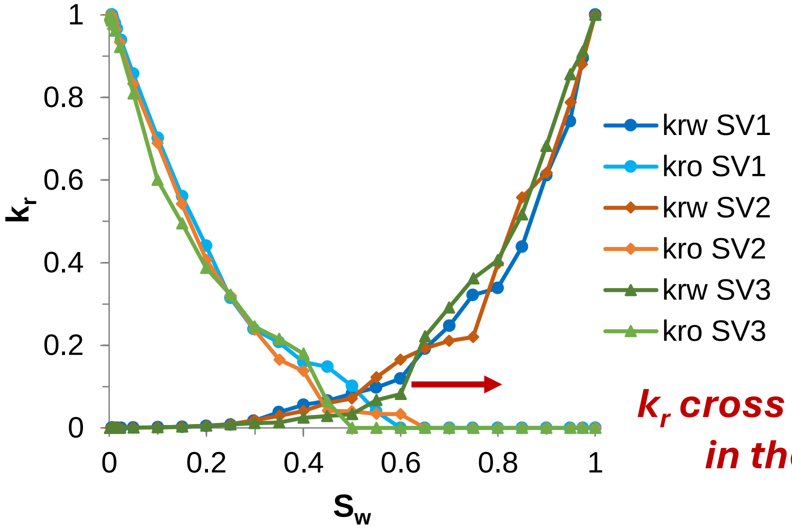


***$k_r$ cross point shifts to the right in the multiscale model***

# Ketton(II) sample (Patmonoaji et al. 2024)

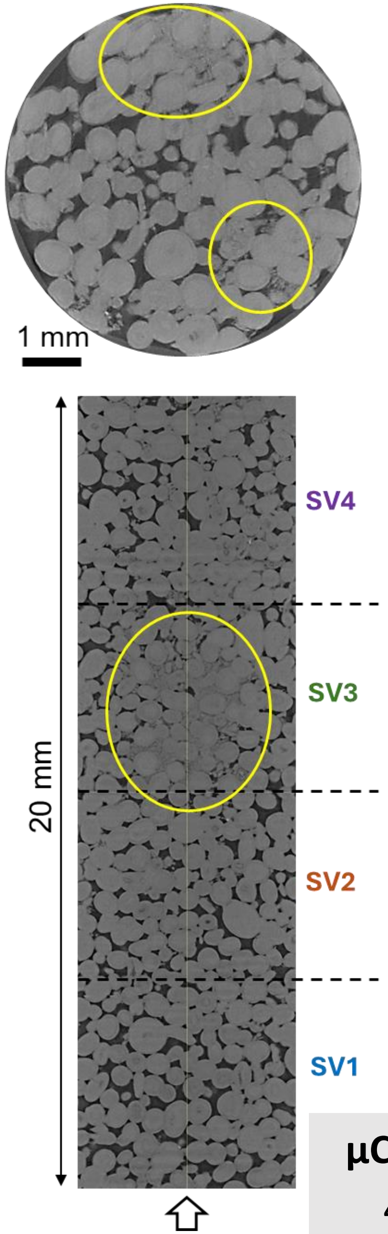


µCT resolution:
4 µm/voxel

- A microporous, more heterogeneous Ketton limestone (calcite-rich)
  - **Helium porosity** = 0.239
  - **Micro-CT porosity** = 0.239
  - **Brine permeability** = 2.233 D
- Microlink determination for four sub-volumes (**1300×1000×1000 voxels**)
- Decane-water drainage by differential imaging-based porous plate method:

**DIPP drainage (decane-water) data:**

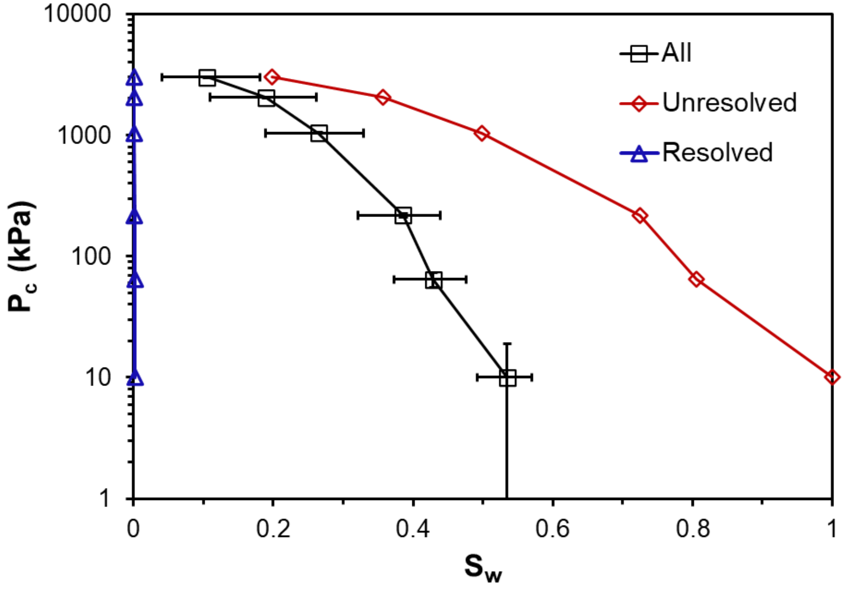


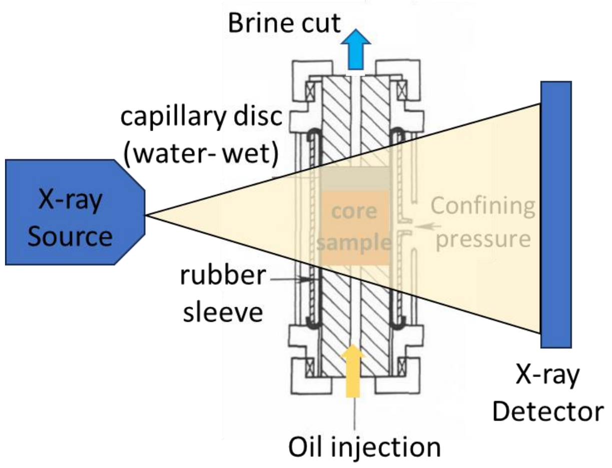


**Schematic representation of the DIPP set-up**

# Ketton(II) sample (Patmonoaji et al. 2024)

- Multiscale GNM results are mostly within the experimental uncertainty region

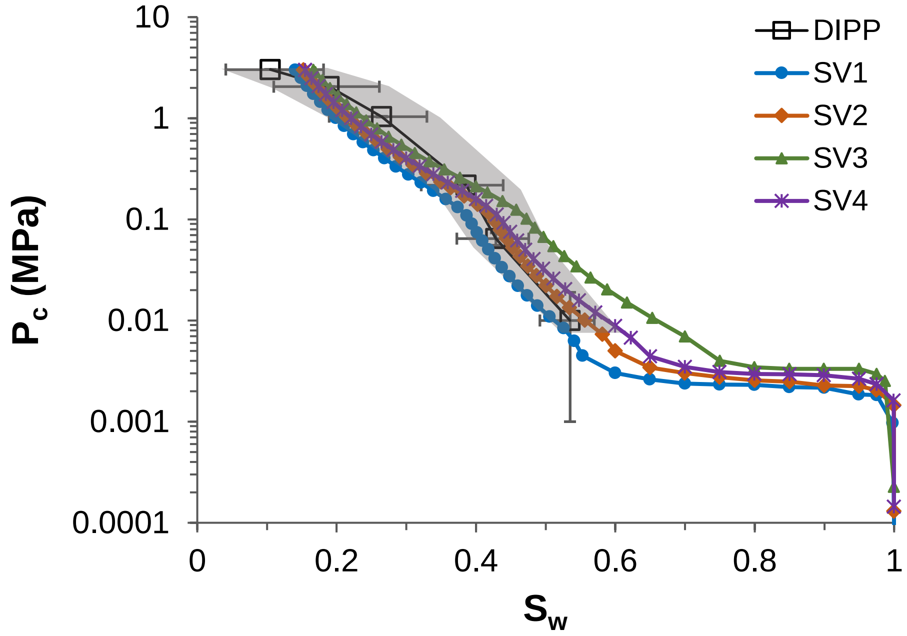


**Tuning parameters:**

| | |
|---|---|
| $d_g$ | $\begin{cases} 30\ \mu m & \phi_m > 0.20 \\ 5\ \mu m & \phi_m \leq 0.20 \end{cases}$ |
| $J_i$ | $\begin{cases} 0.1 & \phi_m > 0.20 \\ 0.2 & \phi_m \leq 0.20 \end{cases}$ |
| $\lambda$ | $\begin{cases} 0.3 & \phi_m > 0.12 \\ 1.4 & \phi_m \leq 0.12 \end{cases}$ |

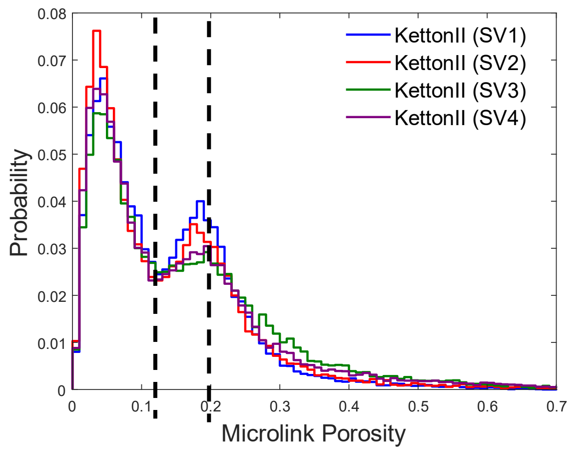


| | Resolved | | | | Multiscale | | | |
|---|---|---|---|---|---|---|---|---|
| | **SV1** | **SV2** | **SV3** | **SV4** | **SV1** | **SV2** | **SV3** | **SV4** |
| $N_p$ | 2410 | 2783 | 2893 | 2933 | 2410 | 2783 | 2893 | 2933 |
| $N_t$ | 4353 | 4251 | 2840 | 3756 | 4353 | 4251 | 2840 | 3756 |
| $N_{mL}$ | – | – | – | – | 15601 | 17570 | 18948 | 19038 |
| $Z$ | 1.81 | 1.53 | 0.98 | 1.28 | 4.58 | 5.13 | 7.67 | 6.07 |
| $\phi$ | **0.14** | **0.113** | **0.073** | **0.10** | **0.258** | **0.237** | **0.225** | **0.236** |
| $K$ [mD] | 7455 | 2994 | 811 | 2241 | 8073 | 3443 | 1127 | **2764** |
| $FF$ | 28.7 | 56.6 | 201.8 | 67.8 | 3.4 | 5.9 | 8.9 | 6.2 |

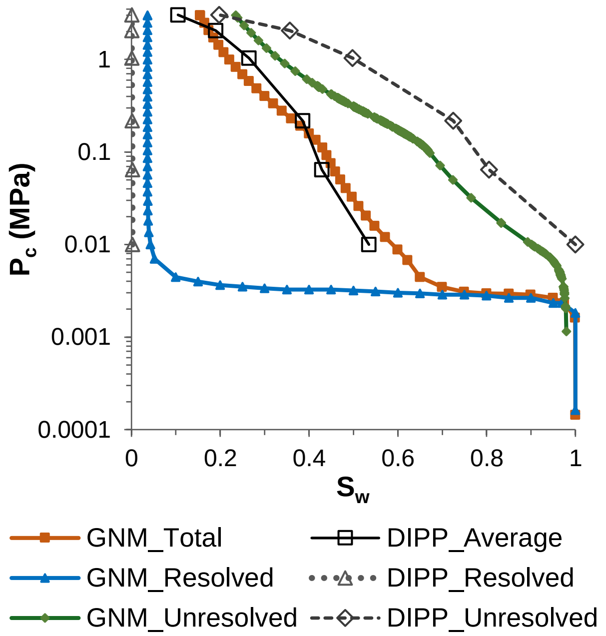


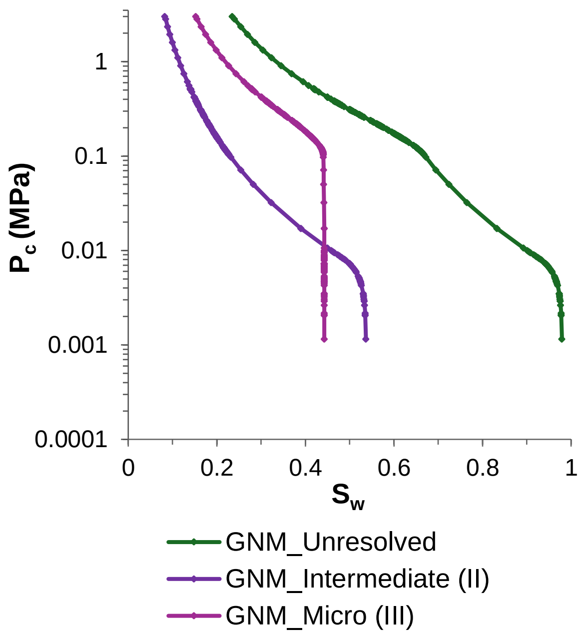

# Ketton(II) sample (Patmonoaji et al. 2024)

- Multiscale GNM results are mostly within the experimental uncertainty region

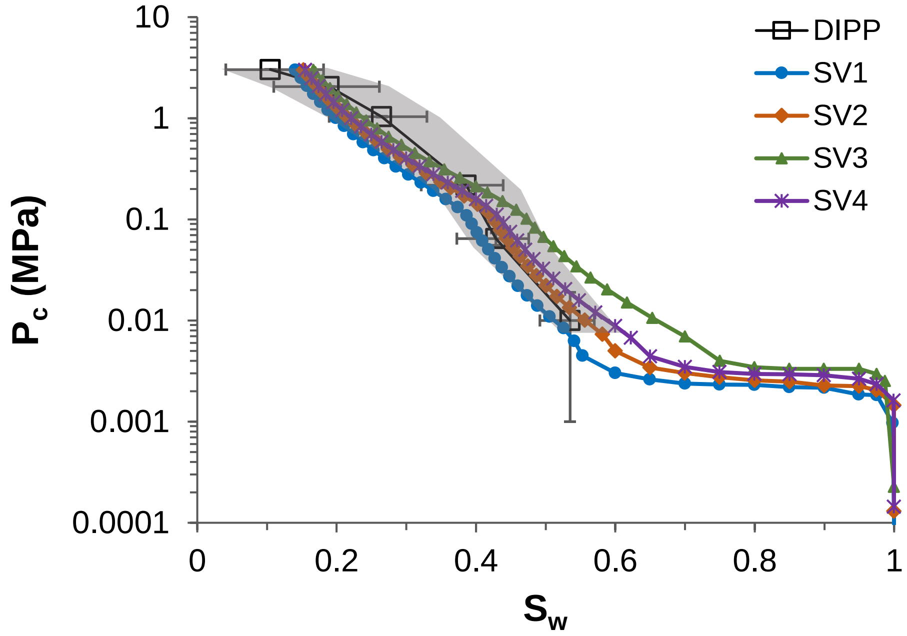


**Tuning parameters:**

| | |
|---|---|
| $d_g$ | $\begin{cases} 30\ \mu m & \phi_m > 0.20 \\ 5\ \mu m & \phi_m \leq 0.20 \end{cases}$ |
| $J_i$ | $\begin{cases} 0.1 & \phi_m > 0.20 \\ 0.2 & \phi_m \leq 0.20 \end{cases}$ |
| $\lambda$ | $\begin{cases} 0.3 & \phi_m > 0.12 \\ 1.4 & \phi_m \leq 0.12 \end{cases}$ |

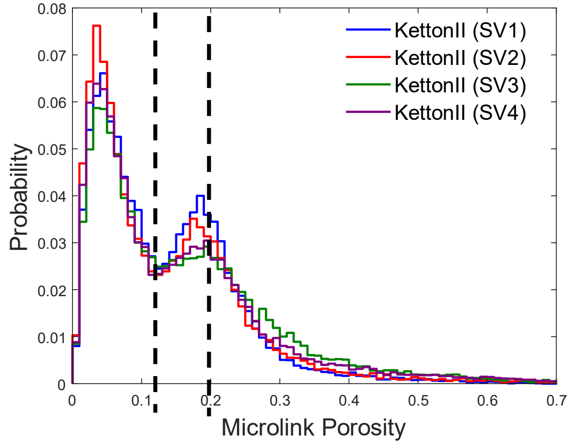


| | Resolved | | | | Multiscale | | | |
|---|---|---|---|---|---|---|---|---|
| | SV1 | SV2 | SV3 | SV4 | SV1 | SV2 | SV3 | SV4 |
| $N_p$ | 2410 | 2783 | 2893 | 2933 | 2410 | 2783 | 2893 | 2933 |
| $N_t$ | 4353 | 4251 | 2840 | 3756 | 4353 | 4251 | 2840 | 3756 |
| $N_{mL}$ | – | – | – | – | 15601 | 17570 | 18948 | 19038 |
| $Z$ | 1.81 | 1.53 | 0.98 | 1.28 | 4.58 | 5.13 | 7.67 | 6.07 |
| $\phi$ | **0.14** | **0.113** | **0.073** | **0.10** | **0.258** | **0.237** | **0.225** | **0.236** |
| $K$ [mD] | 7455 | 2994 | 811 | 2241 | 8073 | 3443 | 1127 | **2764** |
| $FF$ | 28.7 | 56.6 | 201.8 | 67.8 | 3.4 | 5.9 | 8.9 | 6.2 |

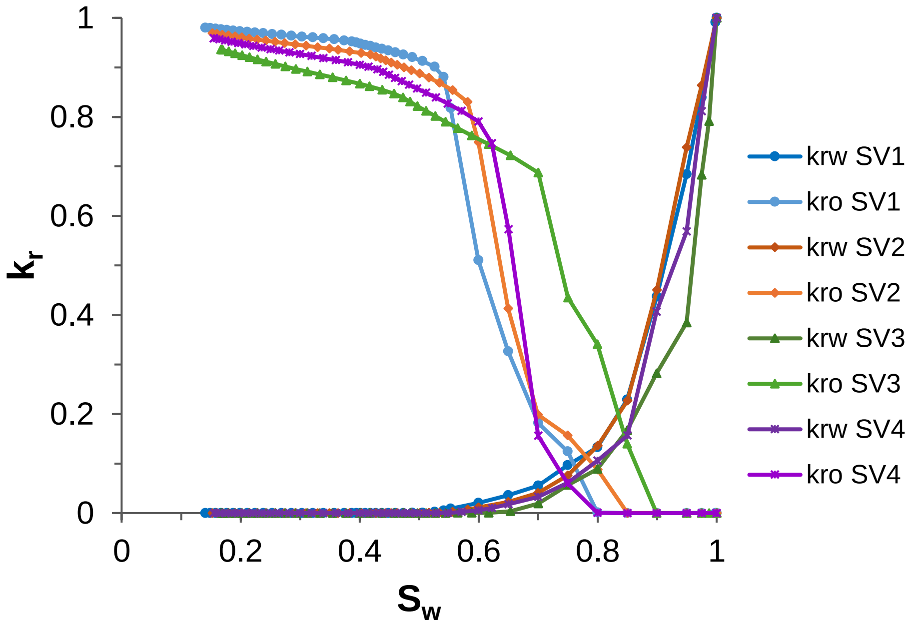

# Enhanced corner connectivity in GNM

- Macro throat corners are the essential pore elements in the GNM
- Corners are connected to their neighbor throats' corners based on the corner proximity

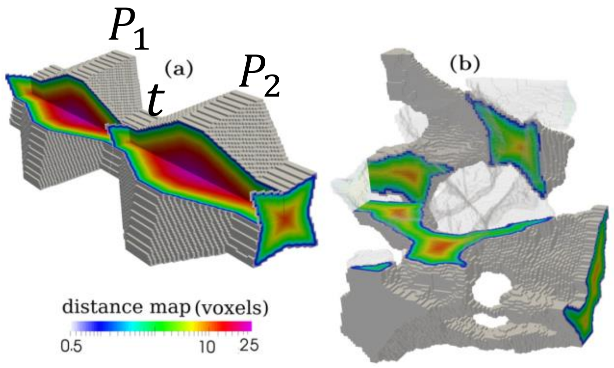


**(Raeini et al., *Phys. Rev. E.*, 2017)**

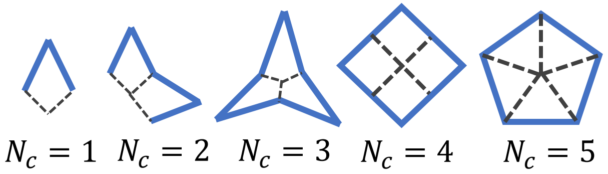


($\boldsymbol{N_c}$ – number of corners per throat)

**Corner connectivity based on directional proximity**

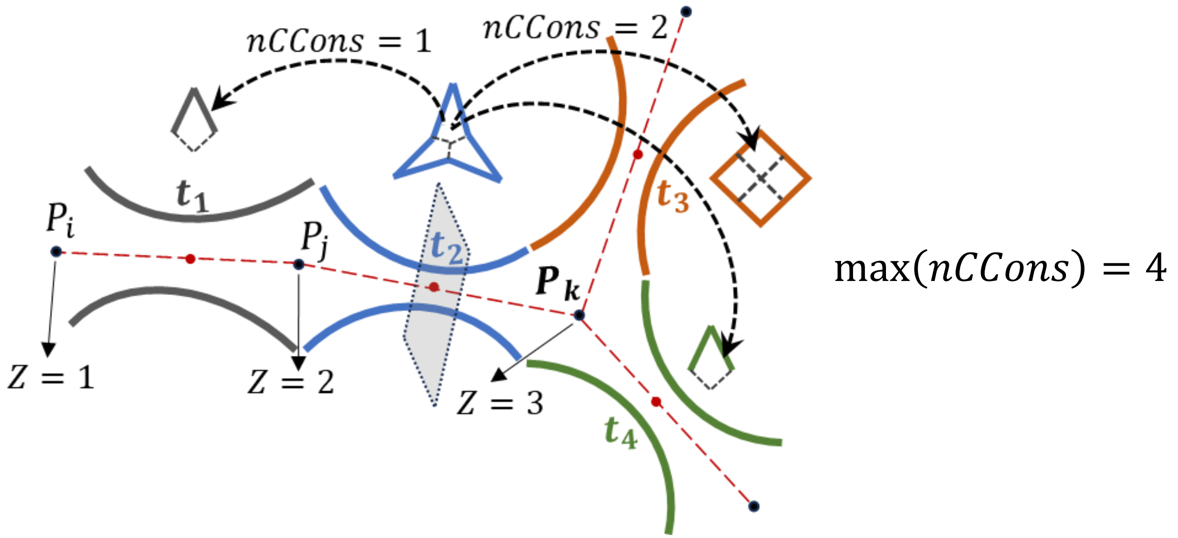


($\boldsymbol{nCCons}$ – number of corner-corner connections)

- For the pore $P_k$: $\boldsymbol{nCCons}$ = [ [__,__,__], [__,__,__,__], [__] ]

$\boldsymbol{N_c} = 3$

$\boldsymbol{t_2}$ $\boldsymbol{t_3}$ $\boldsymbol{t_4}$

$\{0, 1\ or\ 2\}$

# Enhanced corner connectivity in GNM

- For reservoir carbonate, most of the connected throats and throat corners are below the image resolution. This prevents the true connectivity from being represented in the extracted models.

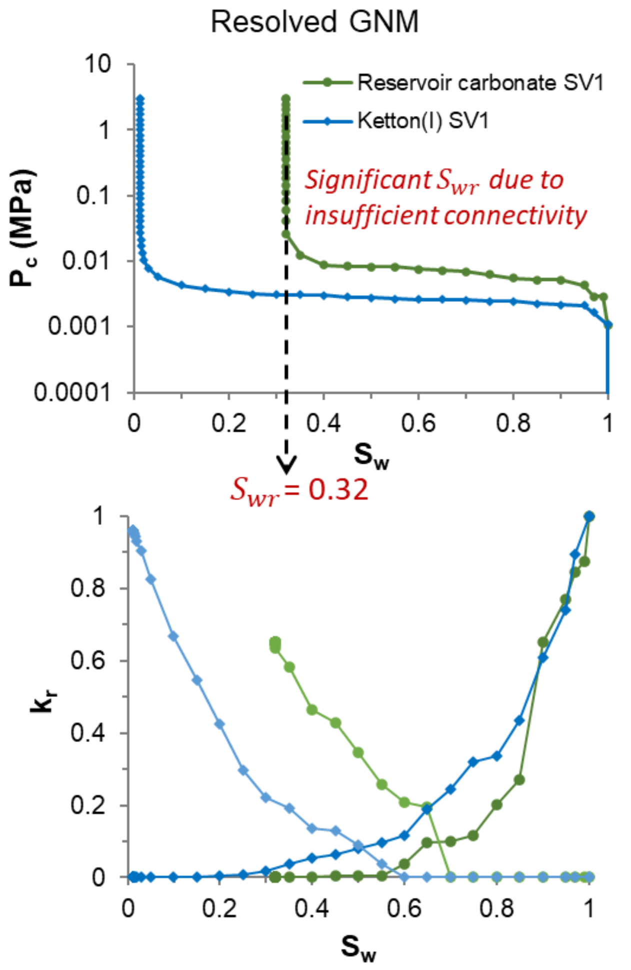


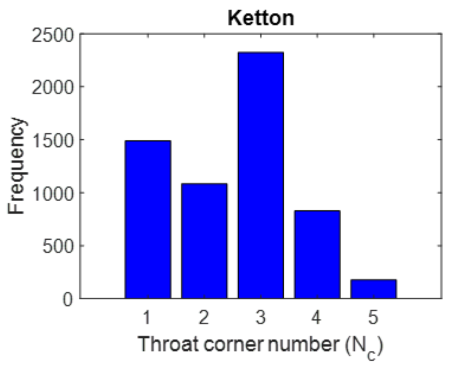


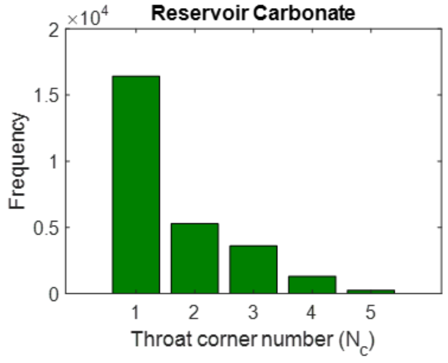


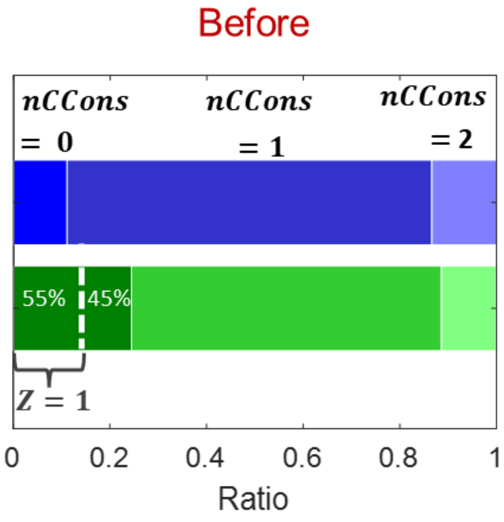


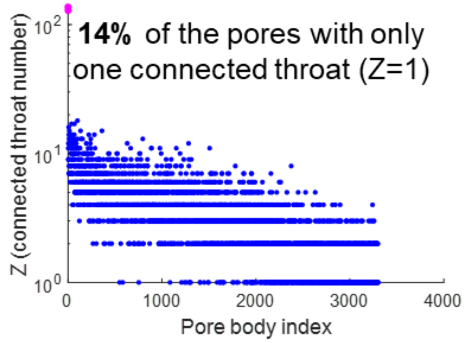


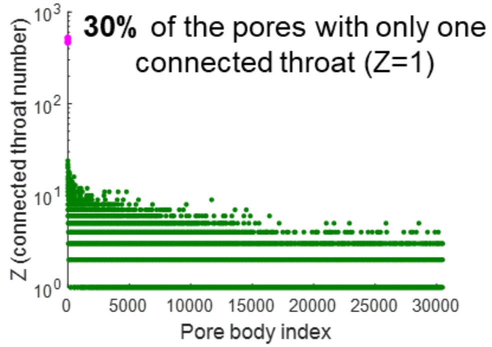


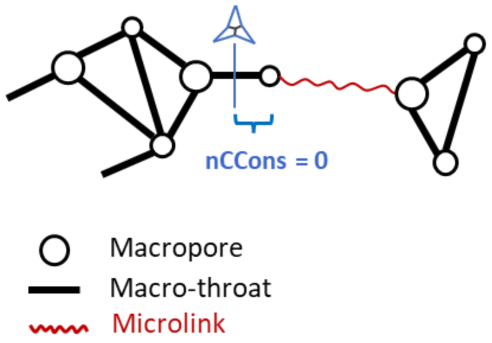

# Enhanced corner connectivity in GNM

- The closest available corners are determined based on their **absolute proximity** which is more inclusive and bidirectional.

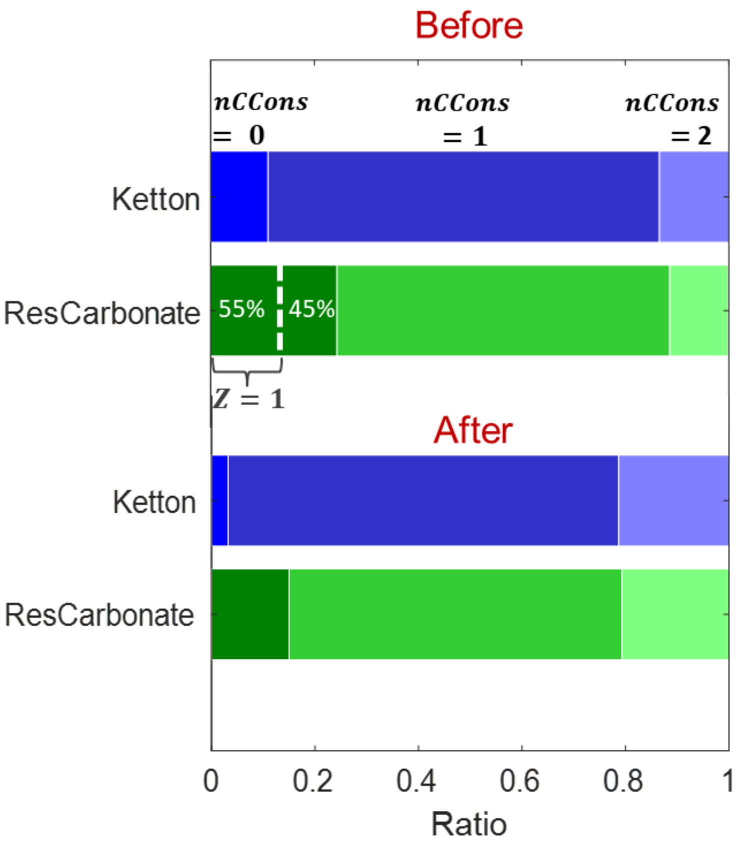


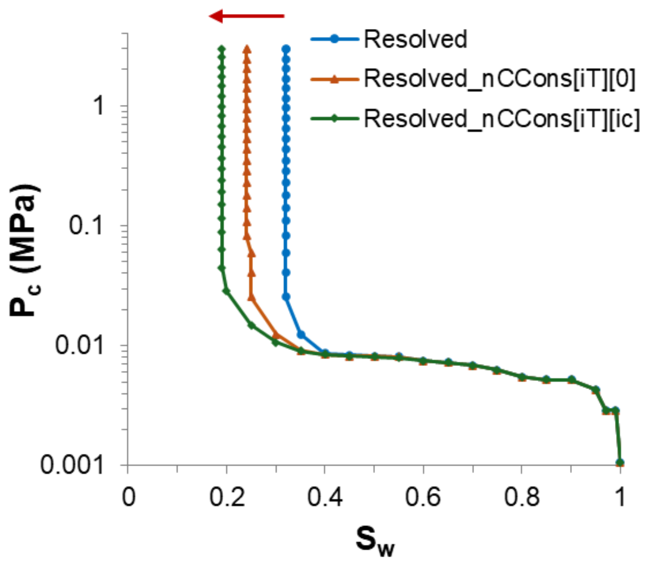


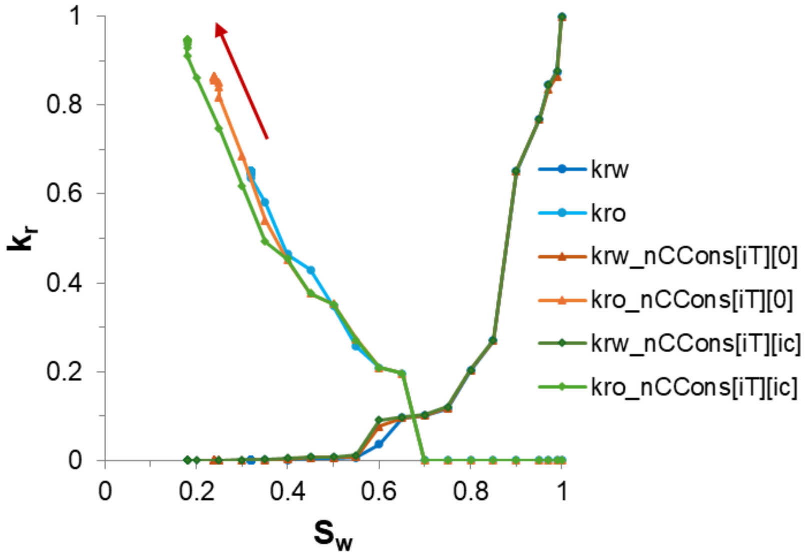


*Less remaining water saturation and greater endpoint oil relative permeability with enhanced corner connectivity in the resolved GNM*

# Reservoir carbonate (Zhang et al. 2023b)

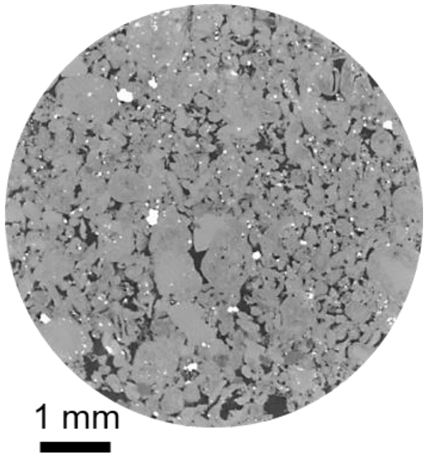


- A complex reservoir carbonate, predominantly limestone and pyrite
  - **Helium porosity** = 0.19
  - **Micro-CT porosity** = 0.188 (**resolved** = 0.073, **unresolved** = 0.115)
  - **Brine permeability** = 88 mD
- Microlink determination for three sub-volumes (**$1120^3$ voxels**)
- Decane-water drainage data from differential imaging-based porous plate experiment:

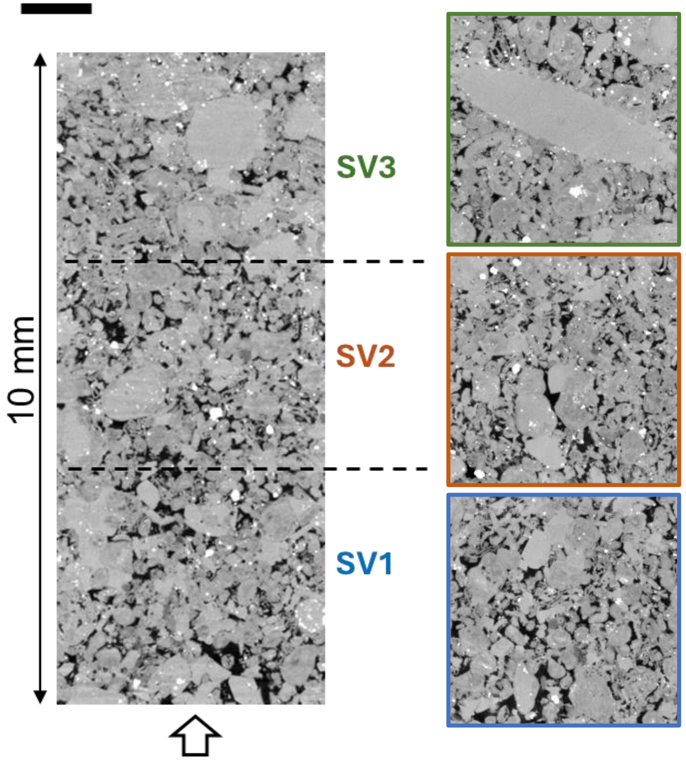


**µCT resolution:**
3.58 µm/voxel

**DIPP drainage (decane-water) data:**

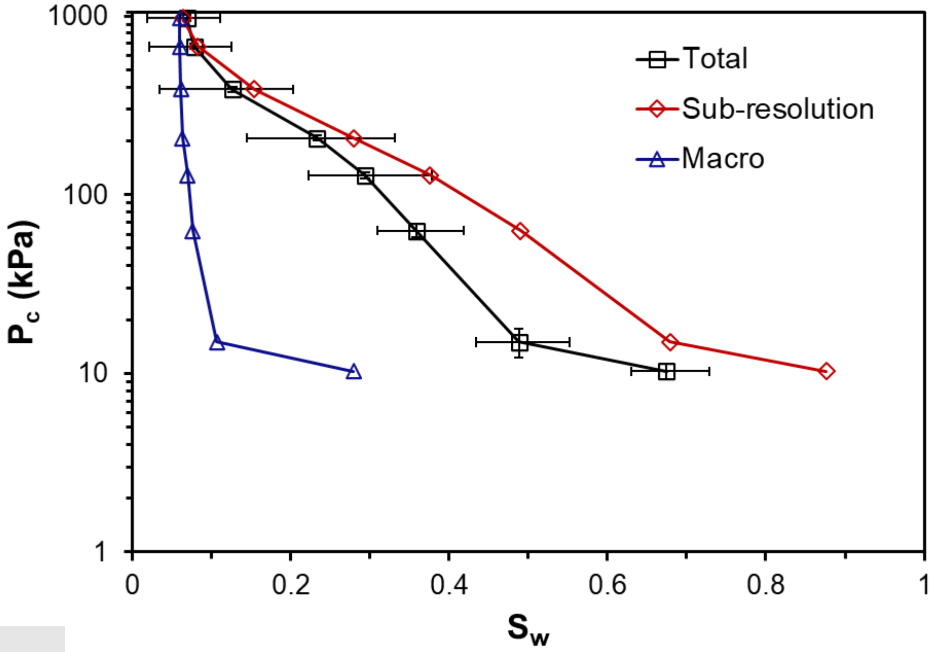

# Reservoir carbonate (Zhang et al. 2023b)

- Multiscale GNM results are mostly within the experimental uncertainty region

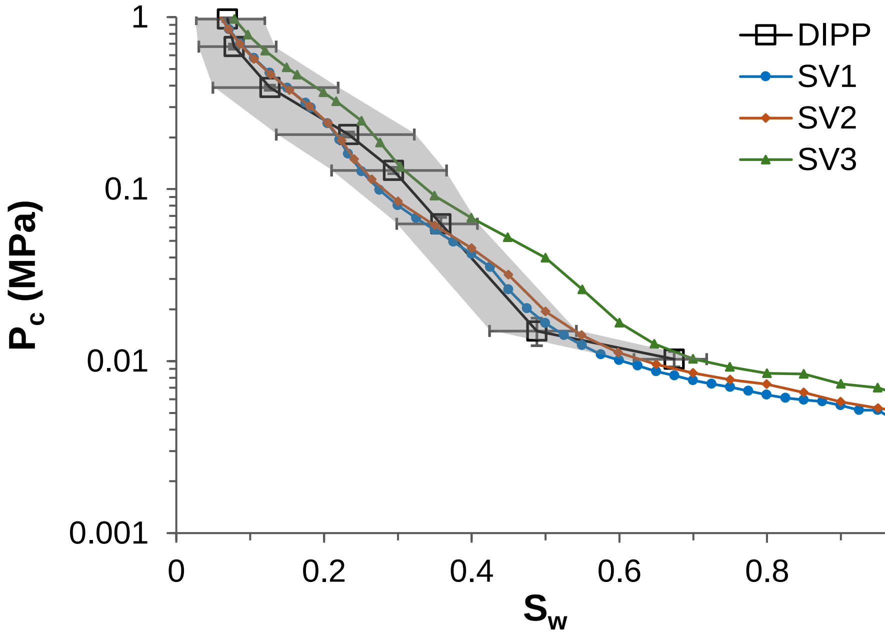


**Tuning parameters:**

| | |
|---|---|
| $d_g$ | $\begin{cases} 18\ \mu m & \phi_m > \phi_{mc} \\ 3\ \mu m & \phi_m \le \phi_{mc} \end{cases}$ |
| $\phi_{mc}$ | $\phi_{mc} = \mathcal{N}(\bar{\phi}_m, \sigma^2)$ |
| $J_i$ | $\begin{cases} 0.1 & \phi_m > 0.25 \\ 0.3 & \phi_m \le 0.25 \end{cases}$ |
| $\lambda$ | 1.0 |

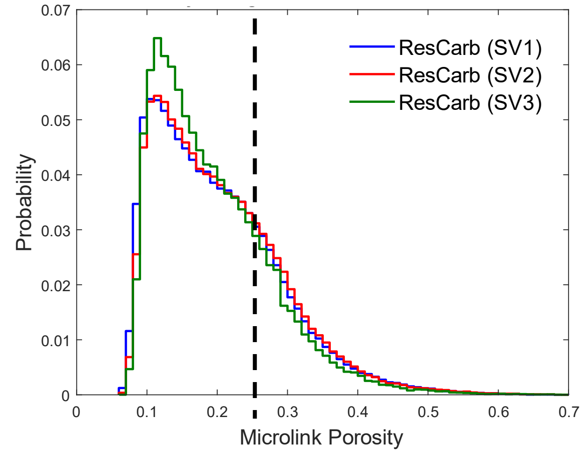


| | Resolved | | | Multiscale | | |
|---|---|---|---|---|---|---|
| | SV1 | SV2 | SV3 | SV1 | SV2 | SV3 |
| $N_p$ | 30508 | 30961 | 25247 | 30508 | 30961 | 25247 |
| $N_t$ | 26897 | 25481 | 19306 | 26897 | 25481 | 19306 |
| $N_{mL}$ | – | – | – | 182805 | 186023 | 155111 |
| $Z$ | 0.88 | 0.82 | 0.76 | 6.87 | 6.83 | 6.91 |
| $\phi$ | 0.082 | 0.072 | 0.05 | 0.209 | 0.205 | 0.170 |
| $K$ [mD] | 52.99 | 14.23 | 2.76 | **90.67** | 37.28 | 9.28 |
| $FF$ | 409 | 1138 | 4308 | 51 | 66 | 133 |

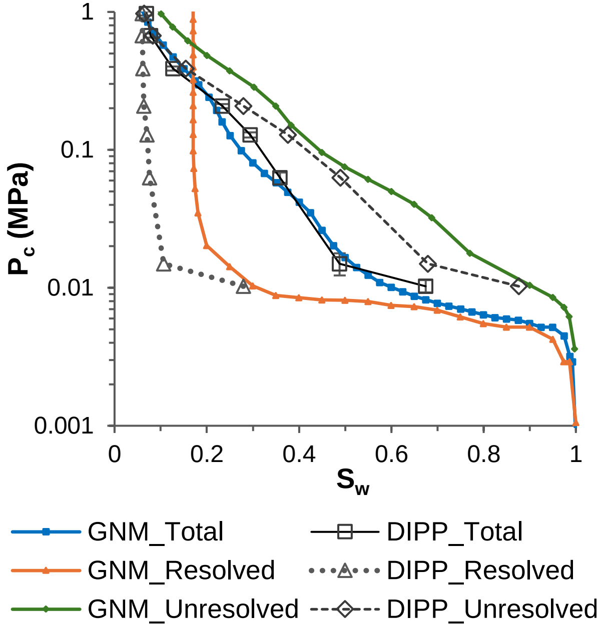


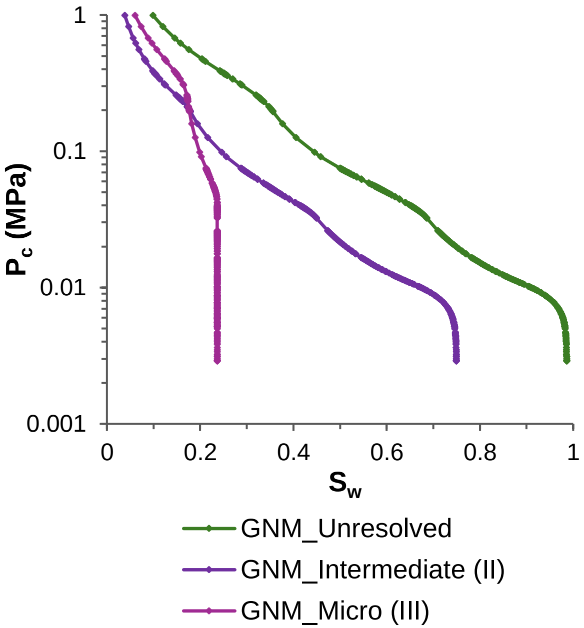

# Reservoir carbonate (Zhang et al. 2023b)

- Multiscale GNM results are mostly within the experimental uncertainty region

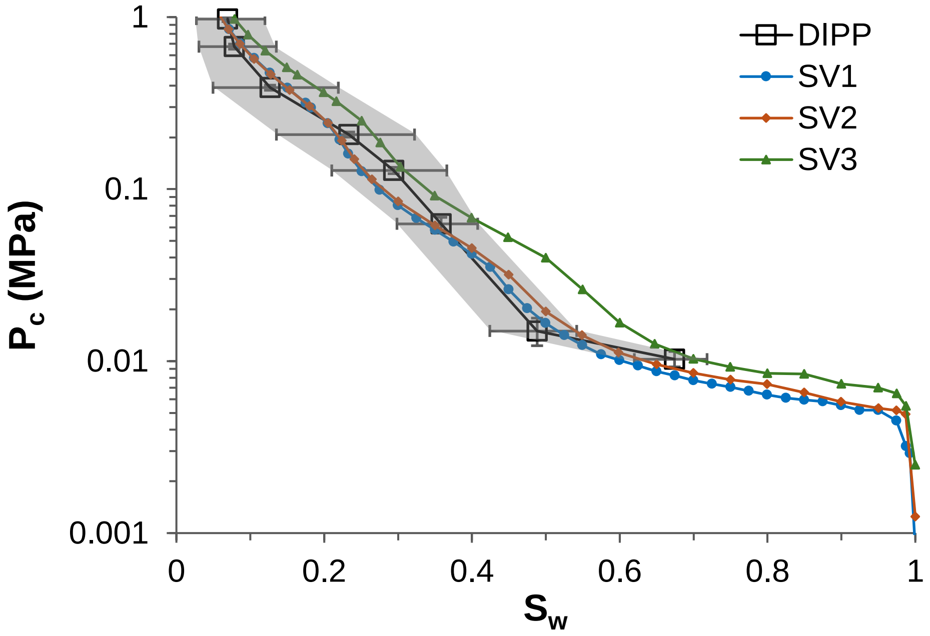


**Tuning parameters:**

| | |
|---|---|
| $d_g$ | $\begin{cases} 18\ \mu m & \phi_m > \phi_{mc} \\ 3\ \mu m & \phi_m \le \phi_{mc} \end{cases}$ |
| $\phi_{mc}$ | $\phi_{mc} = \mathcal{N}(\bar{\phi}_m, \sigma^2)$ |
| $J_i$ | $\begin{cases} 0.1 & \phi_m > 0.25 \\ 0.3 & \phi_m \le 0.25 \end{cases}$ |
| $\lambda$ | 1.0 |

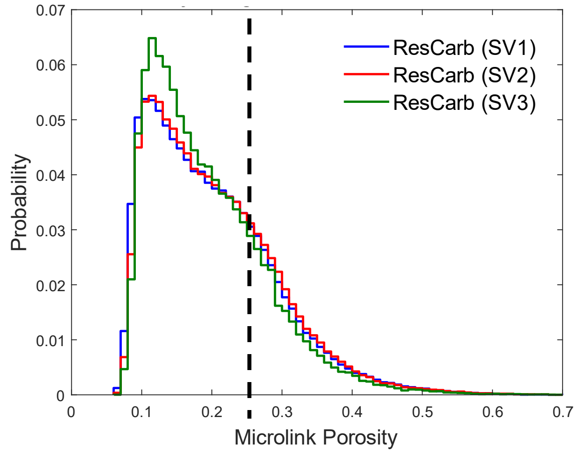


| | Resolved | | | Multiscale | | |
|---|---|---|---|---|---|---|
| | SV1 | SV2 | SV3 | SV1 | SV2 | SV3 |
| $N_p$ | 30508 | 30961 | 25247 | 30508 | 30961 | 25247 |
| $N_t$ | 26897 | 25481 | 19306 | 26897 | 25481 | 19306 |
| $N_{mL}$ | – | – | – | 182805 | 186023 | 155111 |
| $Z$ | 0.88 | 0.82 | 0.76 | 6.87 | 6.83 | 6.91 |
| $\phi$ | 0.082 | 0.072 | 0.05 | 0.209 | 0.205 | 0.170 |
| $K$ [mD] | 52.99 | 14.23 | 2.76 | **90.67** | 37.28 | 9.28 |
| $FF$ | 409 | 1138 | 4308 | 51 | 66 | 133 |

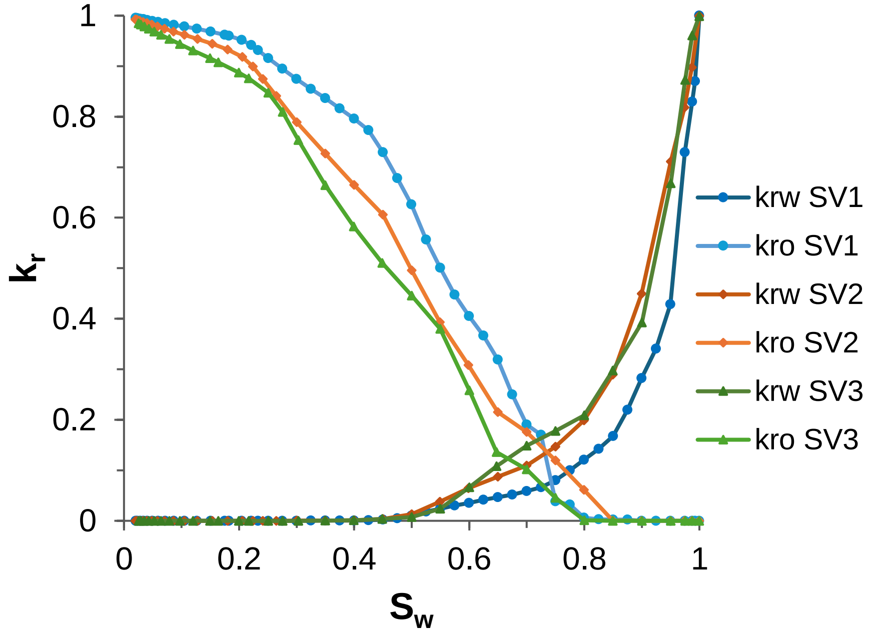

# Summary

- Upscaled properties from the multiscale GNM: absolute permeability and drainage capillary pressure and relative permeability
- Model predictions are within the DIPP experimental uncertainty by effectively using critical empirical parameters
- Improved connectivity in the model with additional porous microlinks and enhanced corner connectivity in complex rocks
- Detailed insights into fluid distribution and continuity across both unresolved and resolved porosity regions

Gundogar, A.S., Foroughi, S., Patmonoaji, A., Regaieg, M., Blunt, M.J. and Bijeljic, B. 2024. **Integration of Unresolved Porosity and Enhanced Connectivity in The Generalized Network Model: Validation Using Pore-Scale Drainage in Heterogeneous Carbonates,** *J. Hydrol.*, Under review.

# Future plans

- Waterflooding in the Multiscale GNM
  - Incorporating wettability characterization in microlinks
  - Investigating trapping behavior in the multiscale system
  - Validation of waterflooding simulations against digital rock experiments
- Darcy-type flow properties of unresolved porosity through direct simulations
- Uncertainties introduced by the unresolved connected porosity representation and flow modeling
- Extending our approach to other complex multiscale systems

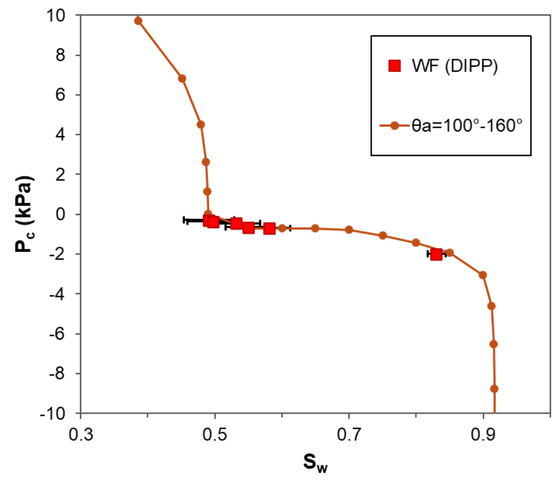


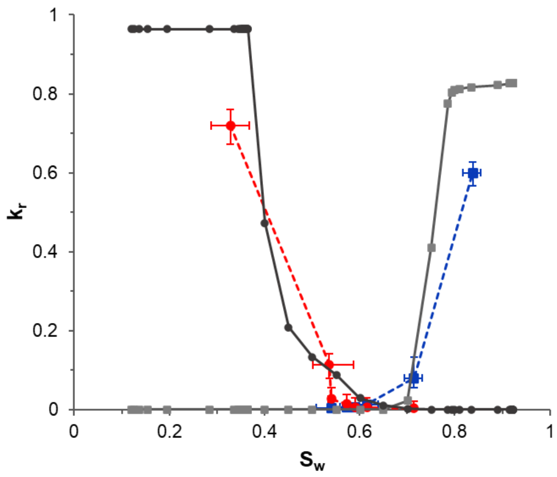

IMPERIAL

# Thank you!

# Questions/Comments?

TotalEnergies

# References


- Raeini, A.Q., Bijeljic, B. and Blunt, M.J. (2017). Generalized network modeling: Network extraction as a coarse-scale discretization of the void space of porous media. Physical Review E , 96 (1), 01331. doi: 10.1103/PhysRevE.96.013312
- Raeini, A.Q., Bijeljic, B. and Blunt, M.J. (2018). Generalized network modeling of capillary-dominated two-phase flow. Physical Review E , 97 (2), 023308. doi: 10.1103/PhysRevE.97.023308
- Blunt, M.J., Bijeljic, B., Dong, H., Gharbi, O., Iglauer, S., Mostaghimi, P., Paluszny, A., and Pentland, C. (2013), Pore-scale imaging and modelling, Advances in Water Resources 51, 197.
- Zhang, G., Foroughi, S., Raeini, A.Q., Blunt, M.J. and Bijeljic, B. (**2023a**). The impact of bimodal pore size distribution and wettability on relative permeability and capillary pressure in a microporous limestone with uncertainty quantification. Advances in Water Resources, 171, p.104352.
- Lin, Q., Bijeljic, B., Foroughi, S., Berg, S. and Blunt, M.J., 2021. Pore-scale imaging of displacement patterns in an altered-wettability carbonate. Chemical Engineering Science, 235, p.116464.
- Lin, Q., Al-Khulaifi, Y., Blunt, M.J. and Bijeljic, B., 2016. Quantification of sub-resolution porosity in carbonate rocks by applying high-salinity contrast brine using X-ray microtomography differential imaging. Advances in water resources, 96, pp.306-322.
- Ghous, A., Senden, T.J., Sok, R.M., Sheppard, A.P., Pinczewski, V.W. and Knackstedt, M.A., 2007, April. 3D characterisation of microporosity in carbonate cores. In SPWLA Middle East regional symposium (pp. SPWLA-MERS). SPWLA.
- Bekri, S., Laroche, C. and Vizika, O., 2005, August. Pore network models to calculate transport and electrical properties of single or dual-porosity rocks. In SCA (Vol. 35, p. 2005).
- Bauer D, Youssef S, Fleury M, Bekri S, Rosenberg E, Vizika O. (2012) Improving the estimations of petrophysical transport behavior of carbonate rocks using a dual pore network approach combined with computed microtomography. Transp Porous Media;94:505–24.
- Bultreys, T., Van Hoorebeke, L. and Cnudde, V., 2015. Multi-scale, micro-computed tomography-based pore network models to simulate drainage in heterogeneous rocks. Advances in Water resources, 78, pp.36-49.
- Ruspini, L.C., Øren, P.E., Berg, S., Masalmeh, S., Bultreys, T., Taberner, C., Sorop, T., Marcelis, F., Appel, M., Freeman, J. and Wilson, O.B., 2021. Multiscale digital rock analysis for complex rocks. Transport in Porous Media, 139(2), pp.301-325.
- Foroughi, S., Bijeljic, B., Gao, Y., & Blunt, M. J. (2024). Incorporation of sub-resolution porosity into two-phase flow models with a multiscale pore network for complex microporous rocks. Water Resources Research, 60(4), e2023WR036393.
- Giudici, L.M., Qaseminejad Raeini, A., Blunt, M.J. and Bijeljic, B., 2023. Representation of Fully Three-Dimensional Interfacial Curvature in Pore-Network Models. Water Resources Research, 59(4), p.e2022WR033983.
- Bijeljic, B., Raeini, A.Q., Lin, Q. and Blunt, M.J., 2018. Multimodal functions as flow signatures in complex porous media. arXiv preprint arXiv:1807.07611.
- Tanino, Y. and Blunt, M.J. Water Resour. Res. 48, W08525 (2012).
- Zhang, G., Regaieg, M., Blunt, M. J., and Bijeljic, B. (**2023b**). Primary drainage and waterflood capillary pressures and fluid displacement in a mixed-wet microporous reservoir carbonate. Journal of Hydrology, 625, 130022.